

Durham Research Online

Deposited in DRO:

19 August 2015

Version of attached file:

Published Version

Peer-review status of attached file:

Peer-reviewed

Citation for published item:

Doyle, R. J and Hirst, D. M. and Hutson, J. M. (2006) 'Ab initio potential energy surfaces, bound states, and electronic spectrum of the Ar-SH complex.', *Journal of chemical physics.*, 125 (18). p. 184312.

Further information on publisher's website:

<http://dx.doi.org/10.1063/1.2371080>

Publisher's copyright statement:

© 2006 American Institute of Physics. This article may be downloaded for personal use only. Any other use requires prior permission of the author and the American Institute of Physics. The following article appeared in *The Journal of Chemical Physics* 125, 184312 (2006) and may be found at <http://dx.doi.org/10.1063/1.2371080>

Additional information:

Use policy

The full-text may be used and/or reproduced, and given to third parties in any format or medium, without prior permission or charge, for personal research or study, educational, or not-for-profit purposes provided that:

- a full bibliographic reference is made to the original source
- a [link](#) is made to the metadata record in DRO
- the full-text is not changed in any way

The full-text must not be sold in any format or medium without the formal permission of the copyright holders.

Please consult the [full DRO policy](#) for further details.

Ab initio potential energy surfaces, bound states, and electronic spectrum of the Ar–SH complex

Richard J. Doyle, David M. Hirst, and Jeremy M. Hutson

Citation: *The Journal of Chemical Physics* **125**, 184312 (2006); doi: 10.1063/1.2371080

View online: <http://dx.doi.org/10.1063/1.2371080>

View Table of Contents: <http://scitation.aip.org/content/aip/journal/jcp/125/18?ver=pdfcov>

Published by the [AIP Publishing](#)

Articles you may be interested in

Highly accurate potential energy surface, dipole moment surface, rovibrational energy levels, and infrared line list for 32S16O2 up to 8000 cm⁻¹

J. Chem. Phys. **140**, 114311 (2014); 10.1063/1.4868327

A three-dimensional ab initio potential energy surface and predicted infrared spectra for the He – N₂O complex

J. Chem. Phys. **124**, 144317 (2006); 10.1063/1.2189227

Spectroscopy of Ar–SH and Ar–SD. II. Determination of the three-dimensional intermolecular potential-energy surface

J. Chem. Phys. **123**, 054325 (2005); 10.1063/1.1943968

Ab initio intermolecular potential energy surface, bound states, and microwave spectra for the van der Waals complex Ne–HCCCN

J. Chem. Phys. **122**, 174312 (2005); 10.1063/1.1888567

The C₃-bending levels of the C₃ – Ar complex studied by optical spectroscopy and ab initio calculation

J. Chem. Phys. **120**, 3189 (2004); 10.1063/1.1641017



Launching in 2016!

The future of applied photonics research is here

OPEN
ACCESS

AIP | APL
Photonics

Ab initio potential energy surfaces, bound states, and electronic spectrum of the Ar-SH complex

Richard J. Doyle^{a)}*Department of Chemistry, University of Sheffield, Sheffield S3 7HF, United Kingdom*

David M. Hirst

Department of Chemistry, University of Warwick, Coventry CV4 7AL, United Kingdom

Jeremy M. Hutson

Department of Chemistry, University of Durham, South Road, Durham DH1 3LE, United Kingdom

(Received 17 August 2006; accepted 29 September 2006; published online 14 November 2006)

New *ab initio* potential energy surfaces for the $^2\Pi$ ground electronic state of the Ar-SH complex are presented, calculated at the RCCSD(T)/aug-cc-pV5Z level. Weakly bound rotation-vibration levels are calculated using coupled-channel methods that properly account for the coupling between the two electronic states. The resulting wave functions are analyzed and a new adiabatic approximation including spin-orbit coupling is proposed. The ground-state wave functions are combined with those obtained for the excited $^2\Sigma^+$ state [D. M. Hirst, R. J. Doyle, and S. R. Mackenzie, *Phys. Chem. Chem. Phys.* **6**, 5463 (2004)] to produce transition dipole moments. Modeling the transition intensities as a combination of these dipole moments and calculated lifetime values [A. B. McCoy, *J. Chem. Phys.* **109**, 170 (1998)] leads to a good representation of the experimental fluorescence excitation spectrum [M.-C. Yang, A. P. Salzberg, B.-C. Chang, C. C. Carter, and T. A. Miller, *J. Chem. Phys.* **98**, 4301 (1993)]. © 2006 American Institute of Physics. [DOI: [10.1063/1.2371080](https://doi.org/10.1063/1.2371080)]

I. INTRODUCTION

van der Waals complexes containing open-shell species are of great current interest. In particular, complexes containing atoms or molecules with orbital angular momentum necessarily involve multiple electronic states.^{1,2} They provide a test bed for studying electronically nonadiabatic effects, which are important in the theory of reaction dynamics.^{3–5} In addition, the observation of prereactive van der Waals complexes trapped in bound levels^{6–10} can shed light on intermolecular forces in the entrance and exit channels of chemical reactions.^{11–14} The form of these shallow, long-range wells can be important in determining reaction outcomes^{15,16} and transition-state geometries.^{17,18}

In this paper, we consider the complex consisting of an open-shell SH radical and an Ar atom. New *ab initio* potential energy surfaces (PESs) for the $X\ ^2\Pi$ state are presented and used in calculations of the bound rotation-vibration levels. We discuss the possibility of employing an approximate approach in the bound-state calculations, using a single adiabatic PES rather than the two surfaces used in the standard method.¹ Finally, the bound-state energies and wave functions are used to simulate the vibrationally resolved electronic spectrum.

The Ar-SH cluster was first detected experimentally by Yang *et al.*¹⁹ using laser-induced fluorescence excitation spectroscopy. Subsequently this group developed empirical PESs for the complex, for both the *A* state²⁰ and the *X* state,²¹ by fitting model functions to reproduce laser-induced fluorescence results. The region of the *A* state PES correspond-

ing to the Ar-S-H configuration (Jacobi angles between $\sim 90^\circ$ and 180°) was determined only approximately, because the fluorescence experiments did not probe this zone. More recently, Hirst *et al.*²² have presented a PES for the *A* state based on *ab initio* calculations at the restricted coupled cluster with single, double, and noniterative triple excitations [RCCSD(T)] level with the aug-cc-pV5Z basis set. This surface was used to predict bound vibrational levels in the Ar-SH configuration²² which have not, to our knowledge, been observed in experiment so far. A possible reason why these levels have eluded detection is discussed in Sec. IV of this paper.

Sumiyoshi *et al.*²³ have recorded high-resolution spectra for Ar-S-H in the ground electronic state using Fourier-transform microwave spectroscopy. These authors also produced PESs for the *X* state based on fitting a function to reproduce their experimental results,²³ and these surfaces were later improved with the aid of some *ab initio* results.²⁴ Most recently, results from microwave-millimeter-wave double-resonance spectroscopy²⁵ were employed to determine new three-dimensional PESs for the *X* state.²⁶

The family of weakly bound clusters containing a rare gas atom and either the OH or SH radical has been reviewed by Carter *et al.*²⁷ in 2000 and by Heaven²⁸ in 2005.

The structure of the present paper is as follows. In Sec. II we present new PESs for Ar-SH ($^2\Pi$) based entirely on *ab initio* calculations at the RCCSD(T) level with an aug-cc-pV5Z basis set. In Sec. III we describe bound rotation-vibration level calculations using these surfaces. We also investigate the wave functions and introduce a new adiabatic approximation for the bound states, including spin-orbit coupling. In Sec. IV the results are combined with those of a

^{a)}Electronic mail: richard.j.doyle@gmail.com

previous study of the $A^2\Sigma^+$ state, in order to produce a high-quality simulation of the vibrationally resolved electronic spectrum.

II. POTENTIAL ENERGY SURFACES

The geometry of the complex is specified in terms of body-fixed Jacobi coordinates r , R , and θ . R is the length of the vector \mathbf{R} which links the center of mass of the SH fragment to the Ar nucleus. The vector \mathbf{r} links the S nucleus to the H nucleus: its modulus r is the SH bond length. The angle between \mathbf{R} and \mathbf{r} is θ , so that $\theta=0^\circ$ corresponds to a linear Ar–H–S configuration. For this work the bond length r was held constant at the experimentally determined equilibrium value of 1.3409 Å,²⁹ which is justified because the vibrational motion of the diatom is very weakly coupled to the relatively low-frequency van der Waals modes of interest.

Energies were calculated for a regular grid of geometry points using the MOLPRO quantum chemistry program.³⁰ These points are at every distance R from 3.25 to 5.5 Å in steps of 0.25 Å and for every angle θ from 0° to 180° in steps of 15° . This gives a total of 130 points. We used the RCCSD(T)^{31,32} method with the aug-cc-pV5Z basis set.^{33–35} The counterpoise procedure of Boys and Bernardi³⁶ was used to correct for basis set superposition error. This is the same level of theory and basis set as were used in recent calculations of the PES for the A state of Ar–SH.²²

Two potential surfaces were obtained from the *ab initio* calculations. These correspond to two adiabatic electronic states: one symmetric (A') and one antisymmetric (A'') with respect to reflection in the plane of the nuclei. The two states are degenerate at linear geometries but nondegenerate at non-linear geometries: the splitting is an example of the Renner-Teller effect. The interaction energies for each state were interpolated using a two-dimensional (2D) spline function, and contour plots of the resulting surfaces are shown in Fig. 1. The A' and A'' surfaces result from the electronic Hamiltonian without spin-orbit coupling. A discussion of surfaces including spin-orbit coupling is presented in Sec. IV.

The adiabatic surfaces (adiabats) are qualitatively similar to those reported for He–SH and Ne–SH complexes.³⁷ The latter were calculated at the RCCSD(T) level, using the smaller aug-cc-pVTZ basis set, but with an additional set of bond functions, and counterpoise correction. A comparison of the positions and energies of the minima on the Ar–SH surfaces presented here with those for X-state He–SH and Ne–SH is given in Table I. For all the A'' surfaces there is a global minimum in the linear X–SH configuration (where X is He, Ne, or Ar) and a local minimum in the linear X–HS configuration. The X–HS configurations are saddle points on the A' surfaces, which have shallow local minima at $\theta=180^\circ$ and global minima at nonlinear configurations. The A' global minima are deeper than those on the A'' surfaces, because in the A' state the SH π hole is directed towards the Ar atom, resulting in reduced repulsion. The global minima for the A' state occur at angles θ that increase with the atomic number of the rare gas atom. Also, as expected, the minima are deeper for clusters containing heavier (and more polarizable) rare gas atoms.

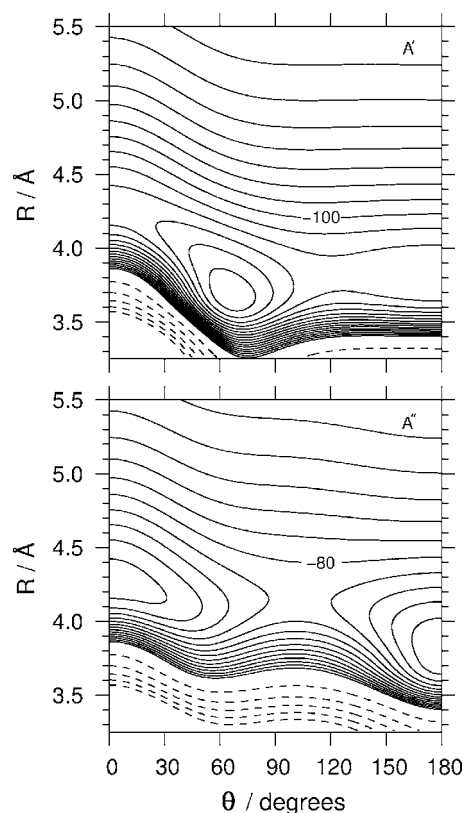


FIG. 1. *Ab initio* potential energy surface contour plots for Ar–SH (X) in the A' state (upper plot) and the A'' state (lower plot). Solid contour lines are shown at 10 cm^{-1} intervals, ranging from 0 to -150 cm^{-1} inclusive for the A' surface and 0 to -120 cm^{-1} inclusive for the A'' surface. Dashed contour lines are shown at 100 cm^{-1} intervals from $+100$ to $+500\text{ cm}^{-1}$ inclusive for both surfaces. The linear Ar–H–S conformation corresponds to $\theta=0^\circ$.

In order to perform dynamical calculations on Ar–SH, we need to evaluate the matrix elements of the potential between electronic states labeled with an angular momentum quantum number λ . For this purpose it is convenient to re-express the PESs as the sum (V_0) and difference (V_2) potentials,

$$V_0(R, \theta) = \frac{1}{2}[V_{A'}(R, \theta) + V_{A''}(R, \theta)],$$

$$V_2(R, \theta) = \frac{1}{2}[V_{A'}(R, \theta) - V_{A''}(R, \theta)].$$

Contour plots of these surfaces are shown in Fig. 2. They are

TABLE I. Positions and well depths of potential minima on the A' and A'' adiabatic surfaces for the X state of SH-rare gas clusters. The results for Ne–SH and He–SH clusters are from Ref. 37.

Cluster	State	R (Å)	θ (deg)	depth (cm^{-1})
Ar–SH	A'	3.678	66.6	157.69
Ne–SH	A'	3.611	57.2	57.05
He–SH	A'	3.639	54.4	25.97
Ar–SH	A' and A''	3.801	180	128.54
Ne–SH	A' and A''	3.593	180	54.27
He–SH	A' and A''	3.593	180	25.27
Ar–SH	A''	4.274	0	125.22
Ne–SH	A''	4.101	0	45.75
He–SH	A''	4.126	0	21.16

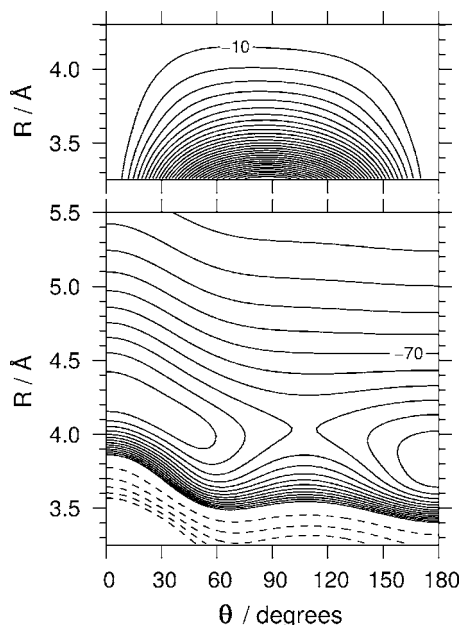


FIG. 2. Contour plots for the Ar-SH (X) difference (upper plot) and sum (lower plot) potential energy surfaces. Solid contour lines are shown at 10 cm⁻¹ intervals, ranging from 0 to -300 cm⁻¹ inclusive for the difference surface and from 0 to -120 cm⁻¹ inclusive for the sum surface. Dashed contour lines are shown at 100 cm⁻¹ intervals from +100 to +500 cm⁻¹ for the sum surface only. The linear Ar-H-S conformation corresponds to $\theta=0^\circ$.

quite similar to those recently presented by Sumiyoshi and Endo.²⁶ The latter were fitted to reproduce experimental results, with starting values for the potential parameters obtained from *ab initio* calculations [RCCSD(T)/aug-cc-pVTZ]. The form of our sum potential is also qualitatively similar to those recently presented for Ne-SH and Kr-SH by Suma *et al.*³⁸

III. BOUND-STATE CALCULATIONS

A. Coupled-channel calculations

The bound states of a complex such as Ar-SH ($X^2\Pi$) involve *both* PESs. In the present work we use a coupled-channel approach to calculate the bound states. In a body-fixed axis system the Hamiltonian operator is

$$H = -\frac{\hbar^2}{2\mu}R^{-1}\left(\frac{\partial^2}{\partial R^2}\right)R + H_{\text{mon}} + \frac{\hbar^2(\hat{J}-\hat{j})^2}{2\mu R^2} + \hat{V}, \quad (1)$$

where H_{mon} is the monomer Hamiltonian and \hat{V} is the intermolecular potential. In a full treatment including overall rotation, the total wave function of the complex may be expanded,¹

$$\Psi_n^{JM} = R^{-1} \sum_{jP\lambda\sigma} \Phi_{jP;\lambda\sigma}^{JM} \chi_{Pn;j;\lambda\sigma}^J(R), \quad (2)$$

where the channel basis functions are

$$\Phi_{jP;\lambda\sigma}^{JM} = \varphi_\sigma \varphi_\lambda \left(\frac{2j+1}{4\pi}\right)^{1/2} D_{P\omega}^{j*}(\phi, \theta, 0) \times \left(\frac{2J+1}{4\pi}\right)^{1/2} D_{MP}^{J*}(\alpha, \beta, 0). \quad (3)$$

The monomer basis functions are labeled by Hund's case (a) quantum numbers λ and σ , the projections of the electronic orbital and spin angular momentum along the SH axis, and $\omega = \lambda + \sigma$.⁵² λ , σ , and ω are all signed quantities. The D functions are Wigner rotation matrices.³⁹ The first D function describes the rotation of the monomer with respect to body-fixed axes, with angular momentum quantum number j (including electronic orbital and spin angular momentum) and projection P along the intermolecular vector \mathbf{R} . The second D function describes the rotation of the complex as a whole, with total angular momentum J and projections M and P onto space-fixed and body-fixed axes, respectively. The angles (β, α) describe the orientation of the \mathbf{R} vector in space.

The monomer Hamiltonian used here for SH($X^2\Pi$) is⁴⁰

$$H_{\text{mon}} = b(\hat{j} - \hat{l} - \hat{s})^2 + H_{\text{so}}, \quad (4)$$

where the rotational constant b is 9.465 cm⁻¹.²⁹ For simplicity the spin-orbit Hamiltonian H_{so} is taken to be independent of R and θ and equal to $a\lambda\sigma$, with $a = -378.5$ cm⁻¹.²⁹

It is convenient to expand the sum and difference potentials in terms of renormalized spherical harmonics $C_{lm}(\theta, \phi)$,

$$V_0(R, \theta) = \sum_l V_{l0}(R) C_{l0}(\theta, 0), \quad (5)$$

$$V_2(R, \theta) = \sum_l V_{l2}(R) C_{l2}(\theta, 0). \quad (6)$$

The potential matrix elements between the angular basis functions may then be written as

$$\begin{aligned} \langle JM; jP; \lambda\sigma | \hat{V} | JM; j'P'; \lambda'\sigma' \rangle \\ = \delta_{PP'} \delta_{\sigma\sigma'} \sum_l V_{l,|\lambda-\lambda'|}(R) g_{l,\lambda-\lambda'}(j\omega; j'\omega'; P), \end{aligned} \quad (7)$$

where the potential coupling coefficients are

$$\begin{aligned} g_{l,\lambda-\lambda'}(j\omega; j'\omega'; P) = (-1)^{P-\omega} [(2j+1)(2j'+1)]^{1/2} \\ \times \begin{pmatrix} j & l & j' \\ -\omega & \lambda-\lambda' & \omega' \end{pmatrix} \\ \times \begin{pmatrix} j & l & j' \\ -P & 0 & P \end{pmatrix}. \end{aligned} \quad (8)$$

The potential matrix elements are independent of J and diagonal in P . Nevertheless, in a full treatment the wave functions of the complex are linear combinations of functions with different values of P , because the operator $(\hat{J}-\hat{j})^2$ in Eq. (1) has matrix elements off-diagonal in P ($\Delta P = \pm 1$). However, the full wave functions are eigenfunctions of the parity operator. Symmetrized basis functions may be constructed by taking even and odd linear combinations of $\Phi_{jP;\lambda\sigma}^{JM}$ and $\Phi_{j-P;-\lambda-\sigma}^{JM}$.

In the present work, the coupled equations are solved

TABLE II. Bound-state energies for $J=3/2$ levels of Ar-SH from full close-coupling calculations (average E_{CC} and parity splitting ΔE_{CC}), helicity decoupling calculations (E_{HD}), and single-surface calculations on the lower adiabatic surface including spin-orbit coupling (E_{ad}). All energies are relative to the dissociation energy to form SH ($X^2\Pi_{3/2}$, $j=3/2$). All energies are given as wave numbers in cm^{-1} .

P	n	E_{CC}	ΔE_{CC}	E_{HD}	E_{ad}
+3/2	0	-102.745	$+3.5 \times 10^{-5}$	-102.652	-102.725
+1/2	0	-97.766	+0.144	-97.593	-97.667
-3/2	0	-94.940	-1.1×10^{-3}	-94.894	-95.035
-1/2	0	-92.116	-0.138	-92.222	-92.293
+3/2	1	-77.292	$+2.6 \times 10^{-5}$	-77.111	-77.258
+1/2	1	-72.276	+0.134	-72.100	-72.148
-3/2	1	-69.356	-1.3×10^{-3}	-69.265	-69.382
-1/2	1	-67.207	-0.124	-67.291	-67.315

using the BOUND program of Hutson.⁴¹ The wave function log-derivative matrix is propagated outwards from a boundary point at short range (R_{\min}) and inwards from a boundary point at long range (R_{\max}) to a matching point (R_{mid}) in the classically allowed region. If E is an eigenvalue of the Hamiltonian, the determinant of the difference between the two log-derivative matrices at R_{mid} is zero.^{42,43} The BOUND program locates eigenvalues by searching for zeros of the lowest eigenvalue of the matching determinant,⁴³ using bisection followed by the secant method. In the present work we use $R_{\min}=3.0$ Å, $R_{\max}=9.5$ Å, $R_{\text{mid}}=4.2$ Å, and a log-derivative sector size of 0.02 Å. The basis set includes all SH functions up to $j_{\max}=15/2$ in both spin-orbit manifolds.

The energies obtained from full close-coupling calculations for the lowest few $J=3/2$ levels of Ar-SH (actually carried out in the equivalent space-fixed basis set¹) are shown in Table II. These levels all correlate with SH $^2\Pi_{3/2}$, $j=3/2$ and are labeled with the projection quantum number P and van der Waals stretching quantum number n . We use the convention that levels in which P and ω for the dominant basis functions have the *same* sign are labeled with positive P and those where they have *different* signs are labeled with negative P .¹ In order of increasing energy, the lowest four levels for Ar-SH have $P=+3/2, +1/2, -3/2, -1/2$, in contrast to Ar-OH where the order is $+3/2, +1/2, -1/2, -3/2$.^{1,44} The difference is due to the anisotropy of the sum potential $V_0(R, \theta)$. The ratio V_{20}/V_{10} is larger for Ar-SH.

The close-coupling results may be compared with the microwave experiments of Sumiyoshi *et al.*,²³ who obtained a rotational constant $B^{\text{eff}}=1569.66$ MHz (0.05236 cm^{-1}) and parity doubling constant $q_J=0.32873$ MHz (1.10×10^{-5} cm^{-1}) for the ground state ($P=+3/2$). These correspond to a $J=3/2-5/2$ separation of 0.262 cm^{-1} and a $J=3/2$ parity splitting of 6.6×10^{-5} cm^{-1} , which compare with calculated values of 0.263 and 3.5×10^{-5} cm^{-1} , respectively. The very good agreement for the rotational spacing suggests that the equilibrium distance of our *ab initio* potential is quite accurate. The difference of almost a factor of 2 in the parity splitting is less satisfactory, but Dubernet *et al.*⁴⁵ have shown that such terms involve complicated combinations of high-order terms involving the difference potential, spin uncoupling, and Coriolis perturbations. Small differences between the energies of excited states can have a large effect on the parity splitting. Sumiyoshi *et al.*²⁵ have very

recently measured microwave-millimeter-wave double-resonance spectra of the $P=+1/2 \leftarrow +3/2$ band of Ar-SH. The center of gravity of the parity components of the $J=3/2 \leftarrow 1/2$ line is 81.8 GHz (2.73 cm^{-1}). The corresponding calculated quantity from our potential is 4.805 cm^{-1} . In addition, the measured parity splitting for the $J=3/2$, $P=+1/2$ level is about 5300 MHz (0.177 cm^{-1}), which compares with 0.144 cm^{-1} from our calculations. An interesting possibility for future work would be to adjust the *ab initio* potential to improve the fit to the spectroscopic parameters using the morphing procedure of Meuwly and Hutson.⁴⁶

B. Wave functions

The full wave functions [Eq. (2)] contain contributions from all possible values of P and ω and are not separable between the body-fixed angles (θ, ϕ) and the space-fixed angles (β, α). This makes them hard to visualize. In addition, since the mixings depend on the total angular momentum J , they are not convenient for calculating band intensities. We therefore introduce two approximations to simplify the description of the wave functions for this purpose. First, we introduce the *helicity decoupling* approximation, where matrix elements of $(\hat{J}-\hat{j})^2$ off-diagonal in P are neglected. Secondly, we neglect matrix elements of H_{mon} off-diagonal in σ (spin-uncoupling terms). The coupled equations then simplify to

$$\left[-\frac{\hbar^2}{2\mu} \frac{d^2}{dR^2} + E_{\omega j}^{\text{mon}} + \frac{\hbar^2}{2\mu R^2} (J(J+1) + j(j+1) - 2\omega^2) - E_{Pn}^J \right] \chi_{Pn;j;\lambda\sigma}^J(R) = - \sum_{j'\lambda'} \langle JM; j' P \lambda' \sigma | \hat{V} | JM; j P \lambda \sigma \rangle \chi_{Pn;j';\lambda'\sigma}^J(R). \quad (9)$$

Since all matrix elements off-diagonal in P and σ have been neglected, states with quantum numbers (P, ω) and $(-P, -\omega)$ are uncoupled and it is not necessary to take combinations of definite total parity. However, states with (P, ω) and $(-P, \omega)$ or $(P, -\omega)$ have different potential energies and are nondegenerate.

The energy levels obtained from helicity decoupling calculations for Ar-SH are included in Table II. The approxi-

mation is accurate to about 0.2 cm^{-1} for $n=0$ and 1 but is less reliable for higher states. In particular, the region between -60 and -40 cm^{-1} contains both $j=3/2$, $n=2$ and $j=5/2$, $n=0$ levels. In the presence of the resulting near degeneracies, the terms that are omitted in the approximate Hamiltonian can cause quite significant level shifts.

In the helicity decoupling approximation, P is a good quantum number. However, ω is not because V_2 mixes levels with $\Delta\lambda=\pm 2$ (but $\Delta\sigma=0$) and thus mixes $\omega=+3/2$ with $-1/2$ and $\omega=+1/2$ with $-3/2$. However, in the absence of terms off-diagonal in σ the two sets are not mixed with one another. Each wave function thus has only *two* components corresponding to different values of ω . The wave functions may be written as

$$\Psi_{Pn}^J = \sum_{\omega} \chi_{Pn;\omega}^J(R, \theta) \Phi_{P;\lambda\sigma}^{JM}, \quad (10)$$

where the basis functions now exclude the θ dependence,

$$\Phi_{P;\lambda\sigma}^{JM} = \varphi_{\sigma} \varphi_{\lambda} \left(\frac{2J+1}{8\pi^2} \right)^{1/2} D_{MP}^{J*}(\alpha, \beta, \phi), \quad (11)$$

and the 2D functions that characterize the components of the wave function for each ω are

$$\chi_{Pn;\omega}^J(R, \theta) = \sum_j \left(j + \frac{1}{2} \right)^{1/2} d_{P\omega}^j(\theta) \chi_{Pn;j;\lambda\sigma}^J(R), \quad (12)$$

where $d_{j\omega}^j(\theta)$ is a reduced rotation matrix.³⁹

We have adapted the BOUND program⁴¹ to calculate wave functions for this case by backsubstituting into the log-derivative propagation equations, as described for the closed-shell (single-surface) case by Thornley and Hutson.⁴⁷ Examples of the resulting wave functions $\chi_{Pn;\omega}^J(R, \theta)$ are shown in Fig. 3. It may be seen that the components for different values of ω have quite different radial and angular distributions.

The Ar-SH wave functions are qualitatively similar to those for Ne-SH obtained by Cybulski *et al.*³⁷ Since the potential anisotropy for Ar-SH is only a few tens of cm^{-1} in the well region, there is only weak mixing of SH rotational functions with different values of j . For this reason the wave functions are dominated by the functions $d_{P\omega}^{3/2}(\theta)$, as described by Dubernet *et al.*¹ for the case of Ar-OH. The d functions are shown, for example, in Fig. 7 of Ref. 1 and the angular parts of the wave functions of Fig. 3 follow them quite closely.

C. Adiabatic approximations

In a basis set of Hund's case (a) functions with signed values of $\lambda=\pm 1$ and $\sigma=\pm 1/2$, we can define new adiabatic surfaces (adiabats) including spin-orbit coupling as eigenvalues of the Hamiltonian matrix at each value of R and θ ,

$$\begin{pmatrix} V_0 + \frac{1}{2}a & 0 & V_2 & 0 \\ 0 & V_0 - \frac{1}{2}a & 0 & V_2 \\ V_2 & 0 & V_0 - \frac{1}{2}a & 0 \\ 0 & V_2 & 0 & V_0 + \frac{1}{2}a \end{pmatrix}, \quad (13)$$

where again the spin-orbit Hamiltonian is taken to be simply $a\lambda\sigma$. This clearly factorizes into two equivalent 2×2 matrices, one containing $\omega=+3/2$ and $-1/2$ and the other containing $\omega=+1/2$ and $-3/2$. The resulting adiabats may be designated $V_+(R, \theta)$ and $V_-(R, \theta)$ with corresponding electronic functions $\psi_+(R, \theta)$ and $\psi_-(R, \theta)$ given by

$$\begin{pmatrix} \psi_+(R, \theta) \\ \psi_-(R, \theta) \end{pmatrix} = \begin{pmatrix} \cos \alpha_{\text{ad}}(R, \theta) & \sin \alpha_{\text{ad}}(R, \theta) \\ -\sin \alpha_{\text{ad}}(R, \theta) & \cos \alpha_{\text{ad}}(R, \theta) \end{pmatrix} \begin{pmatrix} \varphi_{\pm 3/2} \\ \varphi_{\mp 1/2} \end{pmatrix}, \quad (14)$$

where $\varphi_{\omega} = \varphi_{\lambda} \varphi_{\sigma}$. The adiabats for Ar-SH are shown in Fig. 4. Since for Ar-SH $V_2(R, \theta)$ is small compared to a in the well region, the lower adiabat is always predominantly $\omega=\pm 3/2$ in character and the upper adiabat is always predominantly $\omega=\mp 1/2$ in character. The corresponding mixing angle α_{ad} is 0 at $\theta=0^\circ$ and 180° [where $V_2(R, \theta)=0$] and less than 20° at other angles for $R > 3.5 \text{ \AA}$. A contour plot of the mixing angle is shown in Fig. 5.

A further consequence of the large spin-orbit coupling constant is that both adiabats resemble the *sum* potential $V_0(R, \theta)$ much more than the A' and A'' potentials. The spin-orbit coupling has in effect quenched the splitting between the A' and A'' states. This explains why there is no tendency for the wave functions shown in Fig. 3 to "fall into" the nonlinear minimum of the A' state.

The existence of adiabats including spin-orbit coupling suggests a Born-Oppenheimer separation in which the total wave functions are written approximately as

$$\Psi_{iPn} \approx R^{-1} \psi_i(R, \theta) \chi_{iPn}(R, \theta), \quad (15)$$

where ψ_i is one of the functions of Eq. (14) and $\chi_{in}(R, \theta)$ is a solution of an effective Schrödinger equation of the form

$$\left[-\frac{\hbar^2}{2\mu} \frac{\partial^2}{\partial R^2} + H_{\text{rot}} + \frac{\hbar^2(\hat{J} - \hat{j})^2}{2\mu R^2} + V_i(R, \theta) - E_{iPn} \right] \times \chi_{iPn}(R, \theta) = 0. \quad (16)$$

However, the appropriate angular operator H_{rot} to use in such a calculation is hard to define. The reduced rotation matrices $d_{P\omega}^j(\theta)$ that describe the free SH molecule are eigenfunctions of $H_{\text{rot}} = b(\hat{j}^2 - 2\omega^2)$, where

$$\hat{j}^2 = \left[-\frac{1}{\sin \theta} \frac{\partial}{\partial \theta} \left(\sin \theta \frac{\partial}{\partial \theta} \right) + \frac{P^2 + \omega^2 - 2P\omega \cos \theta}{\sin^2 \theta} \right]. \quad (17)$$

This contains singularities at $\theta=0^\circ$ and/or 180° that depend on the values of P and ω . However, there is no single value of ω that is appropriate at all configurations. The simplest approach is to replace ω in Eq. (17) with the value that is appropriate at $\theta=0^\circ$ and 180° and solve Eq. (16) in a basis set of d functions for each value of P . This is equivalent to solving the coupled equations using a basis set containing

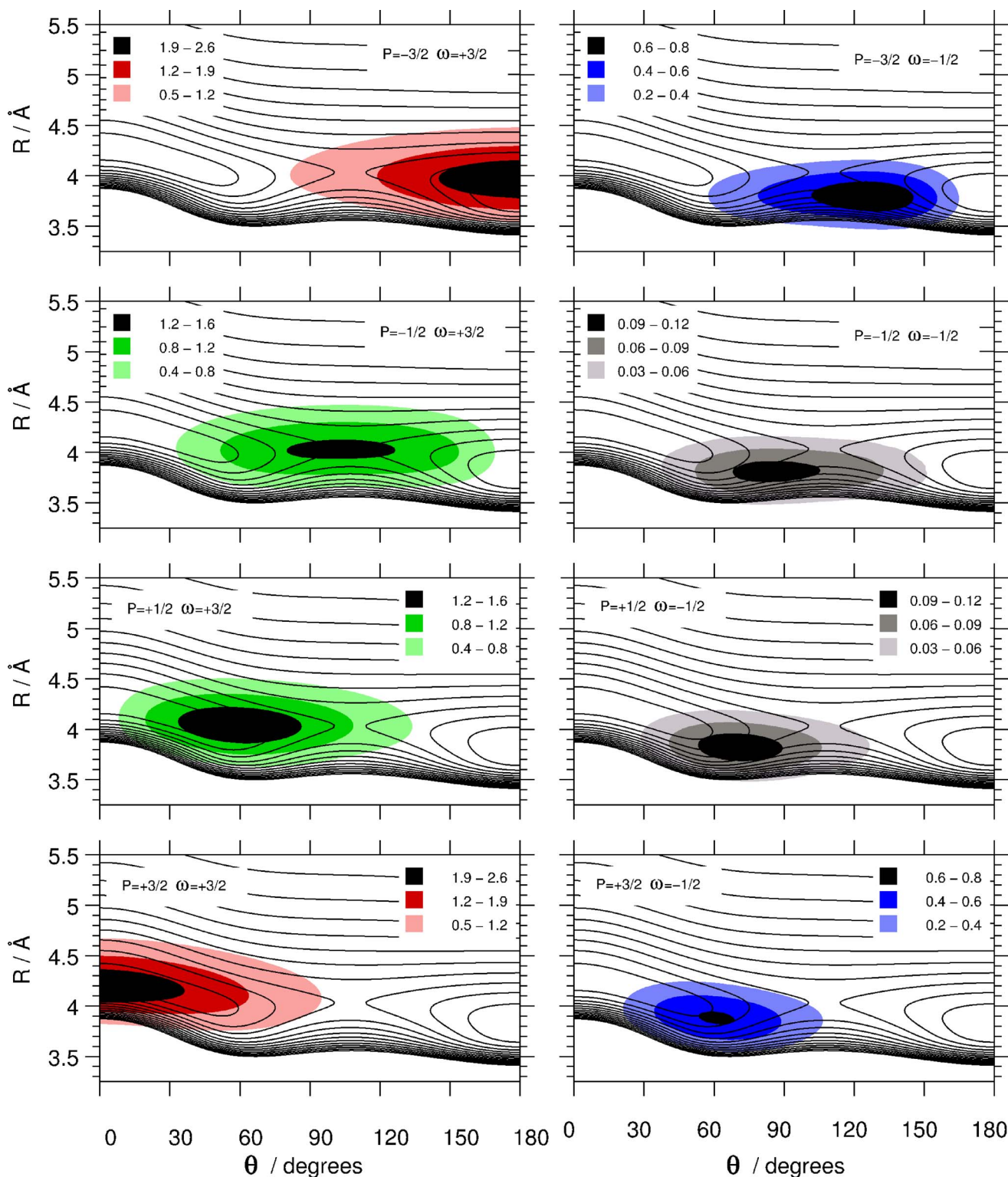


FIG. 3. (Color online) Contour plots of the wave function components, superimposed on the average potential.

only functions with a single value of ω . The results obtained with this approximation are included in Table II. It may be seen that it gives energies that are generally slightly too low (compared to the helicity decoupling results), by $0.05\text{--}0.15\text{ cm}^{-1}$. A slightly better but significantly more complicated approximation would be to replace ω with $\langle\omega\rangle$ and ω^2 with $\langle\omega^2\rangle$ in Eq. (17) to give an improved effective potential.

One approach that is clearly *not* appropriate is to carry out a bound-state calculation on a single adiabat $V_{\pm}(R, \theta)$ assuming that the SH molecule behaves as a closed-shell rigid rotor. Such a calculation would give substantially incorrect energies and wave functions.

It is in fact true that *no wave function of the form (15) can have the correct behavior near both linear geometries*. To see this, consider an alternative definition of the mixing

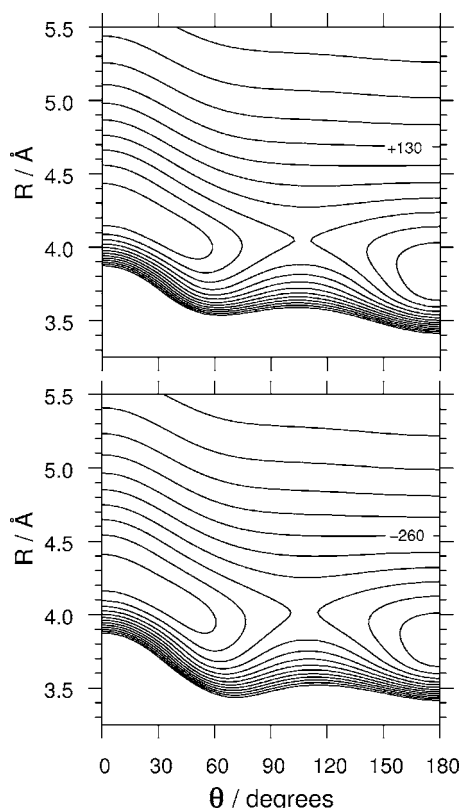


FIG. 4. Contour plots for Ar-SH (X) adiabats including spin-orbit coupling. Contour lines are shown at 10 cm^{-1} intervals, ranging from 70 cm^{-1} to $+a/2$ for the upper surface and from -310 cm^{-1} to $-a/2$ for the lower surface.

angle that can be obtained from a single wave function in the helicity decoupling approximation,

$$\tan \alpha_{Pn}^j(R, \theta) = \frac{\chi_{Pn; \mp 1/2}^j(R, \theta)}{\chi_{Pn; \pm 3/2}^j(R, \theta)}. \quad (18)$$

This quantity is plotted for $n=0$ and all four P values corresponding to $j=3/2$ in Fig. 6. The mixing angles for $P=+3/2$ and $P=+1/2$ bear some similarity to $\alpha_{\text{ad}}(R, \theta)$ (Fig. 5) at small θ , but tend to 90° instead of zero at $\theta=180^\circ$. Conversely, the mixing angles for $P=-3/2$ and $P=-1/2$ tend to 90° at $\theta=0^\circ$. This is easy to explain in terms of the reduced rotation matrices that appear in Eq. (12). For example, the functions $d_{\pm 3/2, \pm 3/2}^j(\theta)$ all behave as $\cos^3(\theta/2)$ as $\theta \rightarrow 180^\circ$, while the functions $d_{\mp 1/2, \pm 3/2}^j(\theta)$ behave as

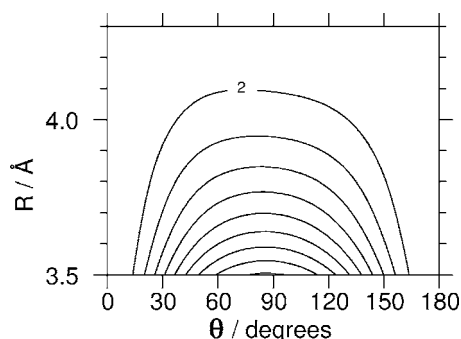


FIG. 5. Contour plot of the adiabatic mixing angle α_{ad} . This angle is derived from the adiabats and is defined in Eq. (14). The contour lines are spaced at 2° intervals.

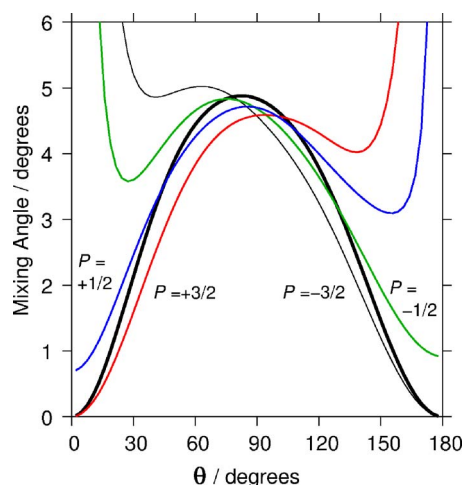


FIG. 6. (Color online) Comparison of the adiabatic mixing angle α_{ad} (thick black line) with angles obtained from wave functions correlating with $j=3/2$, $\omega=+3/2$ for $P=+3/2$ (red), $P=+1/2$ (blue), $P=-1/2$ (green), and $P=-3/2$ (black). The mixing angles are shown as cuts through the corresponding surfaces taken at $R=3.9\text{ Å}$.

$\cos(\theta/2)$. This corresponds to $\tan \alpha_{3/2,n}^j \rightarrow \infty$ as $\theta \rightarrow 180^\circ$ so $\alpha_{3/2,n}^j \rightarrow 90^\circ$ in that limit. The point here is that the component of the $P=+3/2$ wave function on the $\omega=-1/2$ surface goes to zero more slowly than that on the $\omega=+3/2$ surface as $\theta \rightarrow 180^\circ$. Figure 5 shows that the coupled-channel wave functions (10) for $P=+3/2$ and $+1/2$ are predominantly in the $\omega=-1/2$ state near $\theta=180^\circ$, which corresponds to the upper adiabat rather than the lower one. The $P=-3/2$ and $-1/2$ wave functions show similar behavior around $\theta=0^\circ$. This is not the behavior implied by Eq. (15).

IV. ELECTRONIC SPECTRUM CALCULATION

A. Transition wave numbers

In order to calculate the line positions in the vibrationally resolved $A^2\Sigma^+ \leftarrow X^2\Pi$ electronic spectrum, we require the bound-state energies for the excited electronic state, as well as those for the ground state. For the $A^2\Sigma^+$ state we make use of the recent PES presented by Hirst *et al.*²² This surface has a global minimum of -742.5 cm^{-1} at the linear Ar-HS conformation ($\theta=0^\circ$) and a secondary minimum of -673.7 cm^{-1} for linear Ar-SH ($\theta=180^\circ$). The two minima are separated by a barrier more than 600 cm^{-1} high and the lowest-energy vibrational levels are localized within one or the other of the two wells.

The bound states of this PES have been analyzed previously²² and only a brief discussion is given here. Bound-state energies were calculated as eigenvalues of the spin-free triatomic Hamiltonian in Jacobi coordinates. Discrete variable representations (DVRs) were employed for both the intermolecular distance R and the angle θ . For R , 120 sinc-DVR functions⁴⁸ were used, with DVR points ranging from 2.5 to 8.5 Å . For θ , a 64-point DVR based on Legendre polynomials was used. With this basis set, the bound levels of interest were converged to at least seven significant figures. The resulting levels are labeled by quantum numbers (v_{SH}, b^K, n) , where v_{SH} and n are quantum numbers for the SH stretch and the atom-diatom stretch, respectively. K is the

projection of the total angular momentum of the diatom, neglecting spin, onto the body-fixed z axis, and b is the number of nodes in the intermolecular angle θ . The resulting energies for levels with total angular momentum $N=0$ (neglecting spin) are in precise agreement with previous results.²² To facilitate the calculation of band intensities, for $N=1$ the helicity decoupled approximation was employed, in which the Coriolis terms coupling different K levels are ignored. The helicity decoupled energies are within 0.5 cm^{-1} of the full close-coupled results.²²

For the purpose of calculating transition frequencies, the asymptotic separation of the potentials is taken to be the experimental excitation energy from the $v=0, j=3/2$ level of the $^2\Pi_{3/2}$ state to the lowest $v=0, j=1/2$ level of the $^2\Sigma^+$ state of isolated SH, which is $30\,832.68\text{ cm}^{-1}$.⁴⁹ All transitions of the complex were assumed to originate from the $P=+3/2$ level of Ar-SH ($^2\Pi$). The lowest-energy transition frequency for the complex is calculated to be $30\,488.5\text{ cm}^{-1}$, which is 31.5 cm^{-1} greater than the experimental value of $30\,457\text{ cm}^{-1}$.²⁰ This agreement is reasonable, considering the level of theory used in the calculation of the potentials.

B. Transition dipole moments

Calculations of spectroscopic intensities require transition dipole moments $\mu_{\text{tot}}^{\text{if}}$, where

$$\mu_{\text{tot}}^{\text{if}} = \langle i | \mu_{\text{el}} | f \rangle. \quad (19)$$

The integrals involve the initial (i) and final (f) wave functions as determined from bound-state calculations. In this work we evaluated transition dipoles over *internal* coordinates (R, θ), neglecting overall rotation. This gives transition dipoles that correspond to band intensities between intermolecular vibrational states. The electronic dipole moment μ_{el} is in general a parametric function of the nuclear coordinates. In the body-fixed frame it may be expanded in terms of reduced rotation matrices,

$$\mu_{\text{el}}(R, \theta) = \sum_j \mu_{\text{el},j}^{\Delta\lambda}(R) d_{\Delta P, \Delta\lambda}^j(\theta), \quad (20)$$

where $\Delta P = P_i - P_f$ and $\Delta\lambda = \lambda_i - \lambda_f$. In the excited electronic state, $P = K \pm \frac{1}{2}$. In this work it is assumed that μ_{el} consists purely of contributions from the SH monomer, so that only $j=1$ contributes in Eq. (20) and the coefficients $\mu_{\text{el},j}^{\Delta\lambda}$ are independent of R . Since we are dealing with a perpendicular transition in SH, $\Delta\lambda = \pm 1$. The transition dipoles were calculated as one-dimensional Gaussian quadratures in θ , then integrated over R .

C. Intensities and lifetime factors

The signals in a pulsed-laser fluorescence excitation experiment decay exponentially following each pulse, with a lifetime equal to that of the excited state being probed. Intensities are typically measured as the area under the decay curve, and so the experimental intensities are proportional to the lifetime of the excited state. Ar-SH is somewhat unusual in the large range of lifetimes exhibited by different vibrational levels in the A state. It is known that the presence of the Ar atom blocks the electronic predissociation of the SH

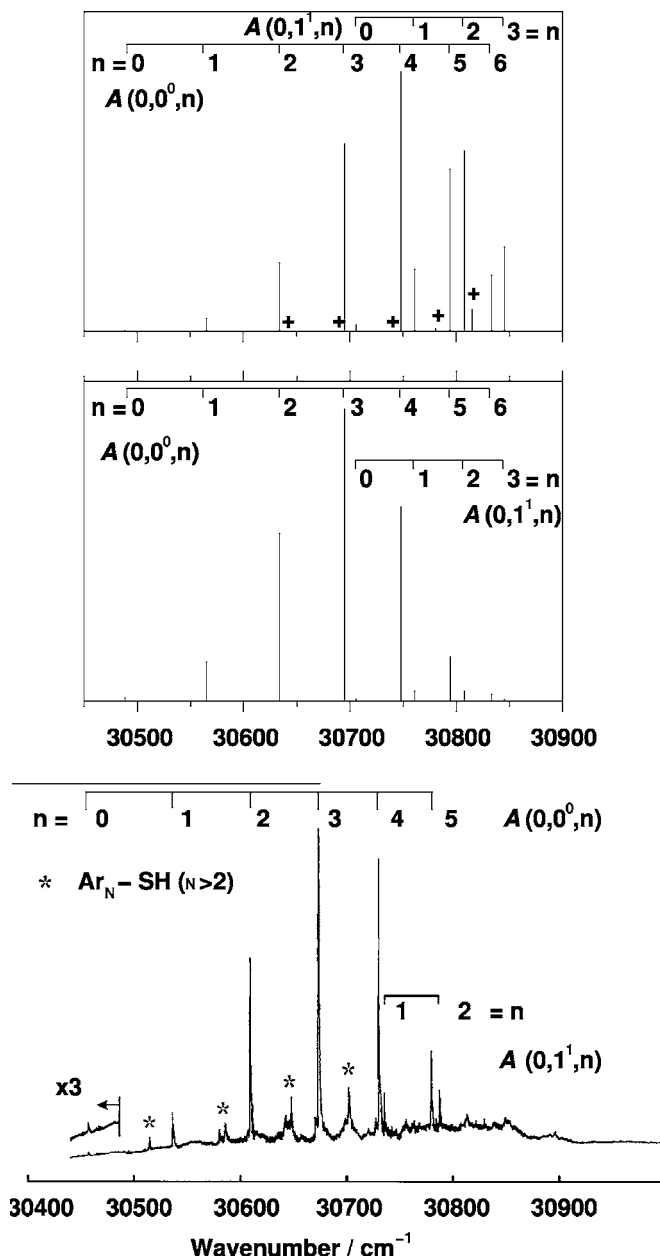


FIG. 7. Calculated vibrationally resolved fluorescence excitation spectrum of Ar-SH for the $A\ ^2\Sigma^+-X\ ^2\Pi$ electronic transition. The lifetime weighting of the intensities is absent for the top panel and present for the middle panel. Lines labeled with + indicate transitions to the $\theta=180^\circ$ well of the A state. For comparison, the experimental spectrum is shown in the bottom panel, taken from Ref. 20. Note that the experimental spectrum contains contributions from $\text{Ar}_2\text{-SH}$ and larger clusters as well as Ar-SH.

radical, leading to a greatly increased lifetime of up to 600 ns for low-lying bound levels, compared to ~ 1 ns for the uncomplexed species.^{20,50} However, the actual lifetime depends on the degree of vibrational excitation, and lifetimes specific to particular levels have been calculated by McCoy.⁵⁰

The top panel of Fig. 7 shows a spectrum calculated directly from the squares of transition dipoles, while the center panel shows a spectrum in which the intensities have been multiplied by McCoy's lifetime values. Clearly this is possible only for levels for which lifetime data exist, and transitions to other levels are omitted in the center panel (i.e.,

it is assumed that their lifetimes are small). Also shown is an experimental spectrum from Ref. 20. The spacings between the peaks in the calculated Ar-SH spectrum are consistently $\sim 5\%$ smaller than in experiment. It is clear that the intensity distributions are significantly different in the two calculated spectra, and that the one that includes lifetime factors gives considerably better agreement with experiment. The agreement in intensities is quite good, especially considering that the experimental spectrum was most likely not normalized for dye laser power.⁵¹ From our results it seems likely that the small peak at $\sim 30\,810\text{ cm}^{-1}$ in the experimental spectrum can be assigned to the transition to $(0,0^{\circ},6)$.

Even without the lifetime weighting, transitions to levels localized in the $\theta=180^{\circ}$ well of the A state, which are labeled with + symbols in Fig. 7, are weak in the simulated spectrum. This arises because of poor overlap with the $P=+3/2$ ground-state wave function (which is concentrated around $\theta=0^{\circ}$). In addition, it is likely that such levels have short lifetimes close to that of uncomplexed SH (Ref. 22) and so will have even lower intensities in the fluorescence excitation spectrum. These levels have not been observed experimentally to our knowledge.

V. SUMMARY

We have obtained new *ab initio* PESs for the Ar-SH complex in its ground $^2\Pi$ electronic state and used them to calculate bound-state energies and wave functions using coupled-channel methods. We have also described a new adiabatic approximation that includes spin-orbit coupling and can be used to calculate bound states on a single PESs. However, the adiabatic wave functions fail to reproduce some features of the true wave functions. We have used our results to simulate the vibrationally resolved laser-induced fluorescence excitation spectrum of Ar-SH, with intensities modeled using calculated transition dipole moments and calculated lifetimes. The inclusion of the lifetime factor is important to obtain satisfactory agreement with the experimental intensities.

ACKNOWLEDGMENTS

The authors would like to thank Terry Miller for providing his experimental spectrum. One of the authors (R.J.D.) also thanks Dr. Stuart Mackenzie for helpful discussions, and is grateful to the Engineering and Physical Sciences Research Council (EPSRC) for funding.

¹M. L. Dubernet, D. Flower, and J. M. Hutson, J. Chem. Phys. **94**, 7602 (1991).

²M. L. Dubernet and J. M. Hutson, J. Chem. Phys. **101**, 1939 (1994).

³M. H. Alexander, G. Capecchi, and H. J. Werner, Faraday Discuss. **127**, 59 (2004).

⁴B. Retail, J. K. Pearce, C. Murray, and A. J. Orr-Ewing, J. Chem. Phys. **122**, 101101 (2005).

⁵M. Ziemkiewicz, M. Wojcik, and D. J. Nesbitt, J. Chem. Phys. **123**, 224307 (2005).

⁶R. A. Loomis and M. I. Lester, Annu. Rev. Phys. Chem. **48**, 643 (1997).

⁷K. Liu, A. Kolessov, J. W. Partin, I. Bezel, and C. Wittig, Chem. Phys. Lett. **299**, 374 (1999).

⁸M. D. Wheeler, D. T. Anderson, and M. I. Lester, Int. Rev. Phys. Chem. **19**, 501 (2000).

⁹M. I. Lester, B. V. Pond, M. D. Marshall, D. T. Anderson, L. B. Harding, and A. F. Wagner, Faraday Discuss. **118**, 373 (2001).

¹⁰J. M. Merritt, J. Kupper, and R. E. Miller, Phys. Chem. Chem. Phys. **7**, 67 (2005).

¹¹M. L. Dubernet and J. M. Hutson, J. Phys. Chem. **98**, 5844 (1994).

¹²M. Meuwly and J. M. Hutson, J. Chem. Phys. **119**, 8873 (2003).

¹³J. Kłos, M. M. Szczesniak, and G. Chałasinski, Int. Rev. Phys. Chem. **23**, 541 (2004).

¹⁴A. V. Fishchuk, P. E. S. Wormer, and A. van der Avoird, J. Phys. Chem. A **110**, 5273 (2006).

¹⁵D. Skouteris, D. E. Manolopoulos, W. S. Bian, H. J. Werner, L. H. Lai, and K. P. Liu, Science **286**, 1713 (1999).

¹⁶T. Xie, D. Wang, and J. M. Bowman, J. Chem. Phys. **116**, 7461 (2002).

¹⁷D. M. Neumark, PhysChemComm **5**, 76 (2002).

¹⁸D. M. Neumark, Phys. Chem. Chem. Phys. **7**, 433 (2005).

¹⁹M.-C. Yang, A. P. Salzberg, B.-C. Chang, C. C. Carter, and T. A. Miller, J. Chem. Phys. **98**, 4301 (1993).

²⁰P. Korambath, X. T. Wu, E. F. Hayes, C. C. Carter, and T. A. Miller, J. Chem. Phys. **107**, 3460 (1997).

²¹M.-C. Yang, C. C. Carter, and T. A. Miller, J. Chem. Phys. **110**, 7305 (1999).

²²D. M. Hirst, R. J. Doyle, and S. R. Mackenzie, Phys. Chem. Chem. Phys. **6**, 5463 (2004).

²³Y. Sumiyoshi, Y. Endo, and Y. Ohshima, J. Chem. Phys. **113**, 10121 (2000).

²⁴Y. Sumiyoshi, Y. Endo, and Y. Ohshima, J. Mol. Spectrosc. **222**, 22 (2003).

²⁵Y. Sumiyoshi, H. Katsunuma, K. Suma, and Y. Endo, J. Chem. Phys. **123**, 054324 (2005).

²⁶Y. Sumiyoshi and Y. Endo, J. Chem. Phys. **123**, 054325 (2005).

²⁷C. C. Carter, H.-S. Lee, A. B. McCoy, and T. A. Miller, J. Mol. Spectrosc. **525**, 1 (2000).

²⁸M. C. Heaven, Int. Rev. Phys. Chem. **24**, 375 (2005).

²⁹K. Huber and G. Herzberg, *Constants of Diatomic Molecules*, Molecular Spectra and Molecular Structure IV (Van Nostrand Reinhold, New York, 1979).

³⁰H.-J. Werner, P. J. Knowles, R. Lindh *et al.*, MOLPRO, Version 2002.6, a package of *ab initio* programs, 2003 (see <http://www.molpro.net>).

³¹P. J. Knowles, C. Hampel, and H.-J. Werner, J. Chem. Phys. **99**, 5219 (1993).

³²P. J. Knowles, C. Hampel, and H.-J. Werner, J. Chem. Phys. **112**, 3106 (1993).

³³T. H. Dunning, Jr., J. Chem. Phys. **90**, 1007 (1989).

³⁴R. A. Kendall, T. H. Dunning, Jr., and R. J. Harrison, J. Chem. Phys. **96**, 6796 (1992).

³⁵D. E. Woon and T. H. Dunning, Jr., J. Chem. Phys. **100**, 2975 (1994).

³⁶S. F. Boys and F. Bernardi, Mol. Phys. **19**, 553 (1970).

³⁷S. M. Cybulski, R. R. Toczyłowski, H. S. Lee, and A. B. McCoy, J. Chem. Phys. **113**, 9549 (2000).

³⁸K. Suma, Y. Sumiyoshi, and Y. Endo, J. Chem. Phys. **120**, 6935 (2004).

³⁹D. M. Brink and G. R. Satchler, *Angular Momentum*, 3rd ed. (Clarendon, Oxford, 1994).

⁴⁰J. M. Brown and A. Carrington, *Rotational Spectroscopy of Diatomic Molecules* (Cambridge University Press, Cambridge, 2003).

⁴¹J. M. Hutson, BOUND computer code, Version 15, 2006.

⁴²B. R. Johnson, J. Chem. Phys. **69**, 4678 (1978).

⁴³J. M. Hutson, Comput. Phys. Commun. **84**, 1 (1994).

⁴⁴M. L. Dubernet and J. M. Hutson, J. Chem. Phys. **99**, 7477 (1993).

⁴⁵M. L. Dubernet, P. A. Tuckey, and J. M. Hutson, Chem. Phys. Lett. **193**, 355 (1992).

⁴⁶M. Meuwly and J. M. Hutson, J. Chem. Phys. **110**, 3418 (1999).

⁴⁷A. E. Thornley and J. M. Hutson, J. Chem. Phys. **101**, 5578 (1994).

⁴⁸D. T. Colbert and W. H. Miller, J. Chem. Phys. **96**, 1982 (1992).

⁴⁹D. A. Ramsay, J. Chem. Phys. **20**, 1920 (1952).

⁵⁰A. B. McCoy, J. Chem. Phys. **109**, 170 (1998).

⁵¹T. A. Miller (private communication).

⁵²We adopt the convention of using lowercase letters for all quantities that refer to monomers and reserve uppercase letters for quantities that refer to the complex as a whole.